NUKLEONIKA 2011;56(2):165–169

ORIGINAL PAPER

Carbon equation of state at high pressure: the role of the radiative transport in the impedance mismatch diagnostics

Abutrab A. Aliverdiev,
Dimitri Batani,
Riccardo Dezulian,
Tomasso Vinci

Abstract. A series of numerical simulation was performed on the application of the impedance mismatch technique to the experimental study of the equation of state (EOS) of porous carbon. Our conclusion is that this technique is useful for such a study up to laser intensities of the order of 10^{14} W/cm^2 (in second or third harmonic of the Nd-laser). However, the inclusion of the radiation transport is important for the correct description of the shock propagation and can affect the results.

Key words: equation of state (EOS) • high pressures • laser shock

A. A. Aliverdiev✉
Institute of Physics,
Daghestan Scientific Centre RAS (DSC RAS),
94 Yaragskogo Str., Makhachkala, Russia
and Dipartimento di Fisica "G. Occhialini",
Università di Milano Bicocca,
Piazza della Scienza 3, I-20126 Milano, Italy,
Tel.: +7 8722 629 070, Fax: +7 8722 628 900,
E-mail: aliverdi@mail.ru, aliverdi@frascati.enea.it

D. Batani, R. Dezulian
Dipartimento di Fisica "G. Occhialini",
Università di Milano Bicocca,
Piazza della Scienza 3, I-20126 Milano, Italy

T. Vinci
Dipartimento di Fisica "G. Occhialini",
Università di Milano Bicocca,
Piazza della Scienza 3, I-20126 Milano, Italy
and Laboratoire pour l'Utilisation des Lasers Intenses,
Ecole Polytechnique,
Palaiseau, France

Received: 22 June 2010
Accepted: 20 September 2010

Introduction

The EOS of carbon at high pressure is a subject of interest for several branches of physics, including astrophysics (a correct description of high-pressure phases is essential for realistic models of planets and stars [13, 22], in particular for the explanation of large magnetic fields of giant planets such as Uranus and Neptune [19, 20]), material science (carbon is a unique element due to its polymorphism and complexity, and a large variety of different phase states), and applied engineering (for example the inertial confinement fusion research).

The important phenomenon of carbon metallization at high pressure had been predicted theoretically, but a convincing experimental demonstration of this effect is still lacking. According to first theoretical estimates [24] the triple point for the transition among diamond, liquid metal, and solid metal should occur at 1.7 Mbar and 3100 K, but this prediction was contradicted by the experiments [11, 23]. More recent works predict a much higher pressure for the metallic transition. At higher temperatures, the presence of liquid phases was predicted, going from non-metallic at low pressure to semi-metallic and metallic at high pressure. The first experimental evidence of a liquid metallic phase was presented in [6, 7]. Nowadays, the most accepted phase diagram of carbon by Grumbach and Martin [12] sets the structural changes in liquid carbon from approximately fourfold to approximately sixfold coordination (metallic liquid) in the pressure range of 4–10 Mbar. This liquid metallic phase may be generated in laboratory conditions using laser-driven shocks. Indeed, the laser-induced ablation and plasma expansion into vacuum result in a material being pushed in the opposite direction, thus generating a shock wave. The

pressure (in Mbar) generated by such shocks can be estimated by [17].

$$(1) \quad P = 11.6(I/10^{14})^{3/4}\lambda^{-1/4}(A/2Z)^{7/16}(Z^{*}t/3.5)^{-1/8}$$

where I is the laser intensity on target in W/cm^2; λ is the laser wavelength in μm; A, Z, and Z^* are respectively the mass number, the atomic number, and the effective ionization degree of the target; and t is the time expressed in ns. According to this formula, the intensities of the order of 10^{14} W/cm^2, which can be obtained quite easily, are sufficient to generate the pressure of the order of 10 Mbar.

An essential complication in the application of laser shocks to the EOS measurements lies in the fact that it is difficult to obtain beams with a uniform high-quality profile and a focal spot-diameter in the order of hundreds of microns. An essential progress in that domain was done only as recently as the 1990's [8, 10, 16]. One of the proposed techniques, which was used in a recent experiment on the porous carbon EOS [4], relies on the application of the phase zone plates (PZP) [16], which eliminate the laser hot spots and provide an almost flat-top laser irradiation profile. Using this technique it is possible to obtain a good planar shock, which may be properly described within the one-dimensional (1D) approximation.

One of the most useful experimental methods for the investigation of the EOS is the so-called impedance mismatch technique, which consists of a simultaneous measurement of the shock velocity for two different materials: the test material with an unknown EOS (which in our case would be carbon), and the reference material, for which the EOS at high pressure is well known (which in our case would be aluminium [14]). The shock-wave measurements are realised by recording the emissivity of the rear side of the shocked target with an appropriate time and space resolution. Using the rear-face time-resolved imaging we can experimentally determine the velocity of the shock propagating through the two steps D_{Al} and D_C, corresponding to particle velocities U_{Al} and U_C, respectively. If the EOS (and hence also the Hugoniot curve) of the reference material (aluminium) is known, we can determine an EOS point for the test material (carbon). In order to find the EOS data point for carbon, we consider the intersection in the (P, U) plane of the line $P = \rho_C D_C U$, where ρ_C is the density of cold carbon, with the reflected shock plotdrawn from the point (P_{Al}, U_{Al}).

A general limitation of the shock-wave EOS experiments is that shocks both compress and heat up the material at the same time, so the pressure and the temperature are not independent variables, and thereby only data on the Hugoniot curve of the material could be obtained. One way to overcome this limitation is to use a target with a reduced density (porous or foam). This changes the initial conditions in the material so that data along different Hugoniot curves may be obtained. In particular, for a reduced initial density of the sample, the same shock pressure P will correspond to a higher temperature T (or internal energy E) and a reduced final density.

Another undesired feature of this method is also the preheating of target caused by secondary X-rays and hot electrons. Such nonlinear physical phenomena take place at laser intensities (I) of the order of $10^{14}/\lambda^2$ W/cm^2, where λ is the laser wavelength expressed in mm. Propagation of the shock wave in an X-ray preheated medium involves several simultaneous processes, including the impact of the X-ray generation on the shock pressure and changes in the shock velocity due to the target rear side expansion. Since hard X-rays and hot electrons are principal causes of the preheating of the material ahead of the shock wave, it is clear that intensities on target above this limit must be avoided in the EOS experiments; however, even for the product $I\lambda^2$ of the order of 10^{13} it is necessary to apply due care in the interpretation of the experimental data [2]. Yet another crucial point is that the stationary conditions for the shock should be necessarily achieved. Otherwise the measured shock velocity does not correspond to the Hugoniot parameters. Although there are many experiments [4, 8, 10, 16] which prove the possibility of creating highly spatially uniform shocks in solids, the analysis of these factors is still an important open problem.

The aim of our work was first to perform a 1D simulation of the processes that occur in multi-layered targets, then to find the "times of shock arrival" for every step of the target, next to reconstruct from these values the carbon EOS, and finally compare it with both the tabulated EOS, used in simulation, and the experimental data. That gives the possibility to: (i) test the tabulated carbon EOS itself, (ii) find the effect of above-mentioned phenomena (preheating and a non-stationary behaviour of the shock) on possible systematic errors in real experiments, (iii) compare the obtained data with recent experimental EOS results obtained for the porous carbon [4] and in this way reduce the systematic error, and finally (iv) tabulate the EOS taking into account new experimental data. In our recent paper [3] we presented the EOS calculated by MQEOS for carbon with reduced density. In this paper we concentrate on the second item on this list, namely the analysis of the effect of preheating and the non-stationary behaviour of the shock on possible systematic errors for the initial laser intensity ~ 10^{13}–10^{14} W/cm^2.

Experiment and simulations

A typical experimental setup commonly used nowadays in the laser-driven EOS experiments with the considered target structure is shown in Fig. 1. This setup is

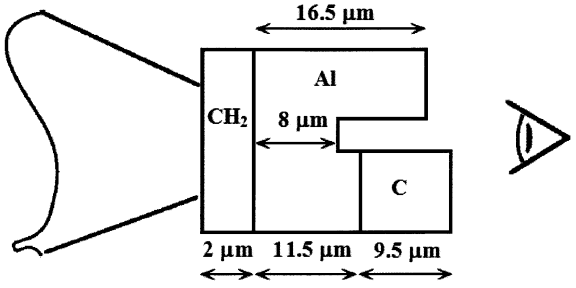

Fig. 1. The target structure. In the real experiments the shock velocities D_{Al} and D_C are determined by measuring the shock travelling times in the step-like material arrangement, using the a visible-light streak camera.

similar to the one used in some recent experiments [4]. The application of the plastic (CH) base layer reduces the amount of X-rays and produces softer, and hence less penetrating X-rays, thus strongly reducing preheating [5]. The simulations discussed in this paper were performed for the second harmonic ($\lambda = 0.526$ μm) of a high-power Nd-laser.

The simulations were performed with the multigroup radiation transport in multilayer foils MULTI [21]. For aluminium we used the SESAME equation of state, for the porous carbon we used the EOS calculated by MPQEOS [15, 18] with a reduced initial density (1.6 g/cm^3) [4] and the SNOP opacities [9]. The flux limiter was taken with the usual value $f = 0.06$, since it is well known that this value can l reproduce experimental results [1] very well.

For each simulation of the experimental EOS investigation by the impedance mismatch technique we realized three different 1D sub-simulations for the following targets: (i) CH-Al (2 + 8 μm), (ii) CH-Al (2 + 16.5 μm), and (iii) CH-Al-C (2 + 11.5 + 9.5 μm). For each of the sub-simulation we determined the time of the shock arrival at the rear target surface. From these three times of arrival we calculated two shock velocities D_{Al} and D_C for aluminium and carbon, correspondingly. Then using the known shock polar and the Hugoniot-Rankine relation for the momentum conservation ($P = \rho DU$) applied to aluminium we found the point

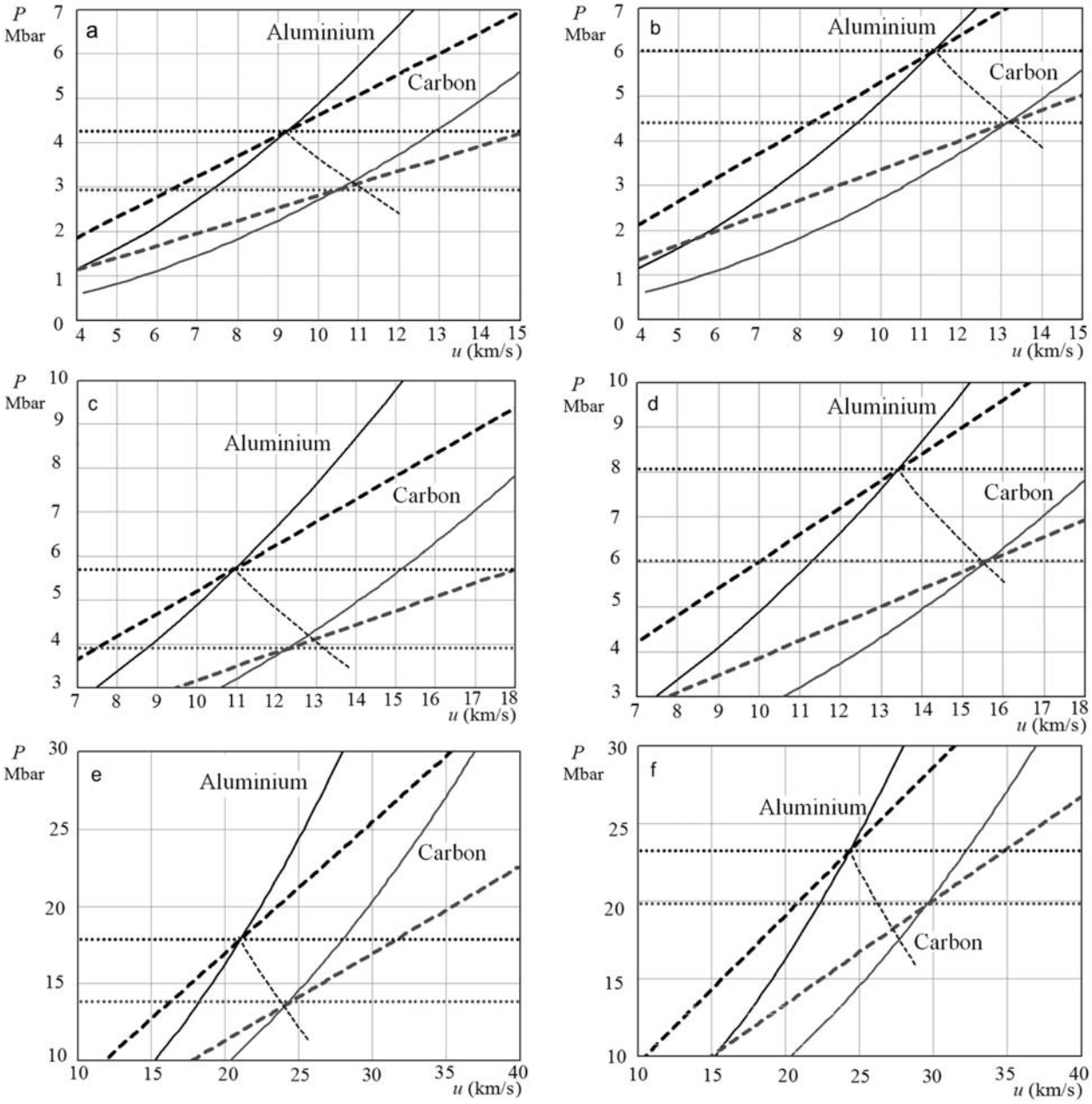

Fig. 2. Shock polars (solid lines) for aluminium and carbon corresponding to the equations of state used in our simulation. The momentum conservation ($P = \rho DU$, dashed lines) corresponds to the shock velocities D_{Al} and D_C obtained from the simulation. The relaxation curve for aluminium is presented by the dotted line. Two horizontal dotted lines correspond to the shock pressure, determined from the intersection of the corresponding polars and the straight lines representing the momentum conservation. The simulation was made without (left) and including (right) the radiation transport, for the initial laser intensity approximately equal to 2×10^{13} W/cm^2 (upper curve), 3×10^{13} W/cm^2 (middle curve) and 2×10^{14} W/cm^2 (lower curve). Gaussian beam profile was assumed, with pulse duration equal to $\tau_{FWHM} = 0.6$ ns.

(U_{Al}, P_{Al}) corresponding to D_{Al}. Finally, using the known relaxation curve for aluminium from the point (U_{Al}, P_{Al}) up to the relation $P = \rho_C D_C U$ (the momentum conservation for carbon) we found the point (U_C, P_C), which should correspond to the shock polar for carbon.

Results and discussion

Figure 2 presents the results of 1D simulation for the initial laser intensity approximately equal to 2×10^{13} W/cm^2 (Figs. 2a and 2b), 3×10^{13} W/cm^2 (Figs. 2c and 2d) and 2×10^{14} W/cm^2 (Figs. 2e and 2f), without (on the left) and including (on the right) the radiation transport. We can see that in almost all cases (except Fig. 2f) we obtained quite good result. The deviation of the intersection point (U_C, P_C) from the polar is on the order of 1–3%, i.e. it is much smaller than a realistic experimental error. The deviation of intersection of the relaxation curve with the straight line representing the momentum conservation is also of the order of few percent, which is less than the usual experimental error in this kind of measurements.

Figure 3 shows the dependences of pressure in the sub-simulations CH-Al-C (2 + 11.5 + 9.5 μm) on the spatial coordinate for a set of time moments. We see that for relatively small intensities of the order of 10^{13} W/cm^2 (upper and middle figures) for simulations not taking into account the radiation transport, the pressure obtained from the shock velocities correspond to the actual shock pressure in each material at least in the first approximation. For the intensity 2×10^{13} W/cm^2 (case Fig. 3a) the

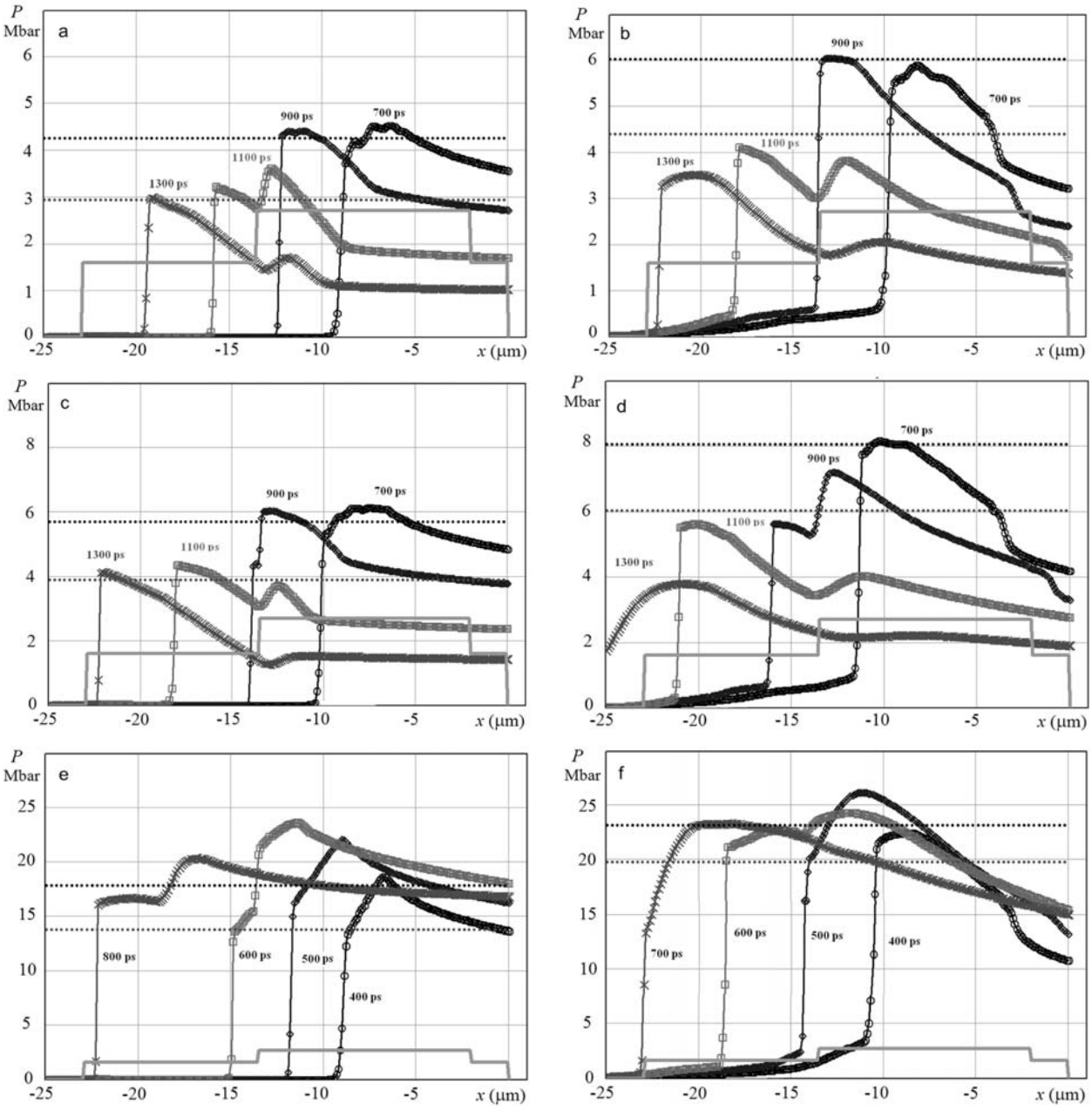

Fig. 3. Pressure as a function of the spatial coordinate, calculated at selected time points. Solid grey rectangular polygon represents the spatial dependence of the initial target density (g/cm^3). The simulation made without (left) and including (right) the radiation transport for the initial laser intensity approximately equal to 2×10^{13} W/cm^2 (upper curve), 3×10^{13} W/cm^2 (middle curve) and 2×10^{14} W/cm^2 (lower curve). Gaussian beam profile was assumed, with pulse duration equal to $\tau_{FWHM} = 0.6$ ns.

shock pressure remains nearly constant for aluminium starting from the end of first aluminium step (–10 μm), and for the whole carbonic part. However, this ceases to be the case already for the intensity of 3×10^{13} W/cm^2, and is definitely not true for 2×10^{14} W/cm^2.

Conclusion

The main conclusion of our work is that shock stationariety is a key parameter for the reliability of results from laser-shock EOS experiments. At high laser intensities (above 10^{14} W/cm^2) and with short-duration laser pulses, this may became a critical assumption which should be carefully checked.

Acknowledgment. We warmly acknowledge the help of colleagues from LULI and PALS in the realization of experiments that served as an input of our numerical analysis. A. A. Aliverdiev is grateful for the financial support from the Landau Network-Centro Volta-Cariplo Foundation, INTAS (06-1000014-5638), ESF (SILMI, 2783), national contract 02.740.11.0397, and RFBR (09-01-96508).

References

1. Aliverdiev A, Batani D, Dezulian R *et al*. (2008) Coronal hydrodynamics of laser-produced plasmas. Phys Rev E 78:046404
2. Aliverdiev A, Batani D, Dezulian R *et al*. (2008) Hydrodynamics of laser-produced plasma corona by optical interferometry. Plasma Phys Control Fusion 50:105013
3. Aliverdiev A, Batani D, Dezulian R, Vinci T (2010) Porous carbon EOS: numerical analysis. Radiation effects and defects in solids: incorporating. Plasma Sci Plasma Technol 165:566–572
4. Batani D, Strati F, Stabile H *et al*. (2004) Data for carbon at megabar pressures. Phys Rev Lett 92:065503
5. Benuzzi A, Koenig M, Faral B *et al*. (1998) Preheating study by reflectivity measurements in laser-driven shocks. Phys Plasmas 5:2410–2420
6. Bundy FP (1973) Diamond synthesis with non-conventional catalyst-solvents. Nature (London) 24:116–118
7. Bundy FP (1989) Pressure-temperature phase diagram of elemental carbon. Physica (Amsterdam) 156A:169–178
8. Collins GW, Da Silva LB, Celliers P *et al*. (1998) Measurements of the equation of state of deuterium at the fluid insulator-metal transition. Science 281:1178–1181
9. Eidmann K (1994) Radiation transport and atomic physics of plasmas. Laser Part Beams 12:223–224
10. Evans AM, Freeman NJ, Graham P *et al*. (1996) Cu Hugoniot measuremets at AWE. Laser Part Beams 14:113–123
11. Grover RJ (1979) "Does diamond melt?" Chem Phys 71:3824–3829
12. Grumbach M, Martin R (1996) Phase diagram of carbon at high pressures and temperatures. Phys Rev B 54:15730–15741
13. Guillot T (1999) Interiors of giant planets inside and outside the solar system. Science 286:72–77
14. Holian KS (ed) (1984) T-4 Handbook of material properties data bases. Vol. 1C: Equations of state. LANL Report no. LA-10160-MS UC-34. Los Alamos National Laboratory
15. Kemp A, Meyer-ter-Vehn J (1998) An equation of state code for hot dense matter, based on the QEOS description. Nucl Instrum Methods Phys Res A 415:674–676
16. Koenig M, Faral B, Boudenne JM *et al*. (1995) Relative consistency of equations of state by laser driven shock wave. Phys Rev Lett 74:2260–2263
17. Mora P (1982) Theoretical model of absorption of laser light by a plasma. Phys Fluids 25:1051–1056
18. More R, Warren KH, Young, DA, Zimmerman GB (1988) A new quotidian equation of state (QEOS) for hot dense matter. Phys Fluids 31:3059–3078
19. Nellis WJ, Hamilton DC, Holmes NC *et al*. (1988) Magnetic fields at Neptune. Science 240:779–781
20. Ness NF, Acuña MH, Burlaga LF *et al*. (1989) The nature of the interior of Uranus based on studies of planetary ices at high dynamic pressure. Science 246:1473–1478
21. Ramis R, Schmalz R, Meyer-ter-Vehn J (1988) MULTI – a computer code for one-dimensional multigroup radiation hydrodynamics. Comput Phys Commun 49:475–505
22. Saumon S, Chabrier G, Van Horn HM (1995) An equation of state for low-mass stars and giant planets. Astrophys J Suppl Series 99:713–141
23. Shaner JW, Brown JM, Swenson DA, McQueen RG (1984) Sound velocity of carbon at high pressures. J Phys (Paris) Colloq 45:235–237
24. Van Vechten JA (1973) Quantum dielectric theory of electronegativity in covalent systems. III. Pressure-temperature phase diagrams, heats of mixing, and distribution coefficients. Phys Rev B 7:1479–1507